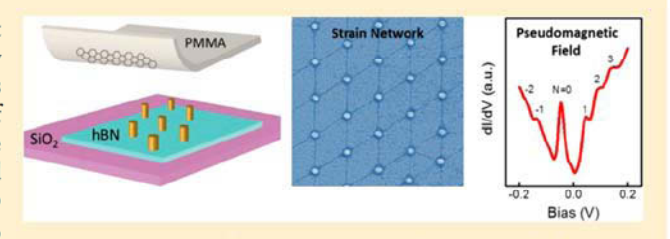


Visualizing Strain-Induced Pseudomagnetic Fields in Graphene through an hBN Magnifying Glass

Yuhang Jiang,^{†,§} Jinhai Mao,^{*,†,§} Junxi Duan,[†] Xinyuan Lai,[†] Kenji Watanabe,[‡] Takashi Taniguchi,[‡] and Eva Y. Andrei^{*,†}

Supporting Information

ABSTRACT: Graphene's remarkable properties are inherent to its two-dimensional honeycomb lattice structure. Its low dimensionality, which makes it possible to rearrange the atoms by applying an external force, offers the intriguing prospect of mechanically controlling the electronic properties. In the presence of strain, graphene develops a pseudomagnetic field (PMF) that reconstructs the band structure into pseudo Landau levels (PLLs). However, a feasible route to realizing,



characterizing and controlling PMFs is still lacking. Here we report on a method to generate and characterize PMFs in a graphene membrane supported on nanopillars. A direct measure of the local strain is achieved by using the magnifying effect of the moiré pattern formed against a hexagonal boron nitride substrate under scanning tunneling microscopy. We quantify the strain-induced PMF through the PLLs spectra observed in scanning tunneling spectroscopy. This work provides a pathway to strain induced engineering and electro-mechanical graphene-based devices.

KEYWORDS: Graphene, nanopillars, strain, distorted moiré pattern, pseudomagnetic field (PMF), scanning tunneling microscopy (STM)

raphene with its two-dimensional (2D) arrangement of atoms in a honeycomb lattice and its suite of unique electronic and mechanical properties^{1,2} carries the promise of realizing flexible, stretchable, and transparent electronics³ that could lead to many potential applications. In particular, its sp² bonded carbon atoms can sustain a record high 25% elastic distortion, making graphene the strongest material known.4 The rearrangement of graphene's atoms in response to strain modifies its low energy band structure and can lead to extremely large strain-induced pseudomagnetic fields (PMFs).5-8 However, the lack of a controllable method to introduce strain⁸ has hindered progress in this area.

A promising configuration for introducing strain in graphene by supporting it on nanopillars 9-13 was recently proposed and studied with spatially resolved Raman spectroscopy, atomic force microscopy (AFM) and scanning electron microscopy (SEM).⁹⁻¹¹ These experiments showed that the strain could be varied by tuning the pillar configuration, their height, and density. But although the strain was found to generate new features in the Raman spectra, no evidence of spectral reconstruction was reported even for strains up to 20%. This raises the question whether such geometry is suitable for manipulating graphene's band structure. Here we revisit this issue by combing SEM, AFM, scanning tunneling microscopy (STM), and scanning tunneling spectroscopy (STS) to investigate strain-induced PMFs in a graphene membrane stretched over a nanopillar array. STM measurements of the distorted moiré pattern produced by strained graphene resting on an hexagonal boron nitride (hBN) substrate in between pillars provided a direct measure of the local strain. The magnifying effect¹⁴ of the moiré pattern makes it possible to detect strain levels that are otherwise below the instrumental resolution. At the same time, the appearance of clear pseudo Landau levels (PLLs) in the strained regions afford direct and quantitative evidence of the strain-induced PMF.

Figure 1a illustrates the sample fabrication steps (details in SI) designed to induce a strain network in the graphene membrane covering the nanopillars. 12,13 Two types of pillar materials were used: an insulator, lift-off resists (LOR), and a

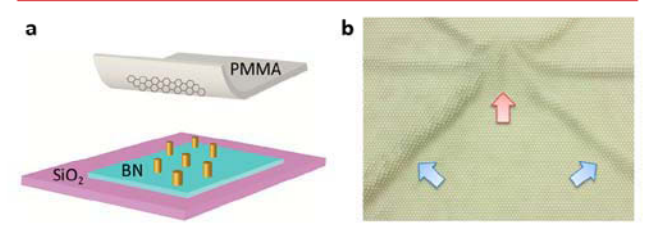


Figure 1. Schematics of device fabrication. (a) Stacking graphene on the pillared substrate. (b) Schematics of graphene supported on a pillar (red arrow) and the strain-induced ripples (blue arrows).

Received: December 16, 2016 Revised: April 4, 2017 Published: April 14, 2017

Department of Physics and Astronomy, Rutgers University, Piscataway, New Jersey 08854, United States

^{*}Advanced Materials Laboratory, National Institute for Materials Science, 1-1 Namiki, Tsukuba 305-0044, Japan

conductor, Au. Following the fabrication of the pillar array, a single layer of graphene is deposited on the pillars with a thin poly(methyl methacrylate) (PMMA) sacrificial film using the standard dry transfer method. 15 The PMMA film provides rigidity to the graphene/PMMA structure so that it remains suspended even after being transferred onto the pillar array. Subsequently, the removal of the PMMA film with solvent produces a strong capillary force between the graphene membrane and the substrate. 16 The final result is a distorted three-dimensional graphene lattice with conical singularities at the pillar positions. Stress radiates outward from the pillars producing strain that results in a graphene wrinkle network (Figure 1b), similar to the well-known wrinkling in thin elastic membranes. 17-20 Depending on the aspect ratio of the pillar array, this procedure can result in either a suspended graphene canopy or a collapsed graphene membrane resting on the substrate between pillars. 10 However, in both the suspended and supported configurations the graphene membrane is subjected to a nonuniform distribution of strain that is expected to produce PMFs. 13 The pillar arrays were triangular with periods in the range $1-2 \mu m$ and height range of 50-600 nm.

Following the fabrication, samples are characterized at room temperature by optical microscopy, SEM (30 kV acceleration voltage) and by AFM topography in the semicontact mode. The samples are then annealed overnight in forming gas (9:1, Ar to $\rm H_2$ ratio) at 230 °C in order to remove the PMMA residue prior to the STM/STS measurements at 4.6 K. In STS, the $\rm dI/dV$ spectra providing a measure of the local density of states (LDOS) (I is the tunneling current, V is the sample bias) are measured by the standard lock-in technique with an alternating current (ac) voltage modulation ($V_{\rm RMS} = 4$ mV, f = 473.1 Hz) added to the direct current (dc) bias.

We first explore the sample supported on the LOR pillared structure. Figure 2a shows the optical micrograph of graphene on the prepatterned LOR pillars (600 nm height and 1 μ m period). In this case, the pillars are first patterned using standard SEM lithography by overdosing the LOR, but the pattern is not developed in order to keep a flat surface for the coming graphene transfer (see SI for details). Next, the graphene membrane is stacked on top of the undeveloped LOR substrate by a dry transfer process. Finally, the LOR between the pillars is removed with an ethyl-lactate developer followed by exposure to nitrogen gas flow for drying. The evaporation of the solvent that fills the gap between the graphene and the substrate generates a strong capillary force causing the graphene membrane to collapse toward the substrate.

Figure 2b shows a top view SEM image of the graphene (light green) on LOR pillars (bright spots) after the developer step. We note that the graphene flake was torn in two after the development, providing a vivid illustration of the huge deformation strain generated during the collapse process. The AFM topography image (inset in Figure 2b) shows sagging of the graphene membrane in between pillars. Interestingly, we note that the collapse of the membrane introduces a network of strain-induced ripples linking each pillar to its neighbors.

Turning to Figure 2c, we observe that the LOR pillars adjacent to the tear in the graphene flake are visibly bent out of shape as they are pulled apart by the two torn pieces. The bent pillars provide a strikingly visual confirmation of the strain in this system. A 45° angle side view (Figure 2d) directly illustrates the bent pillars at the edge of the flake (blue arrow). In contrast, the pillars outside the graphene covered regime (yellow arrows) remain upright and undistorted (yellow line).

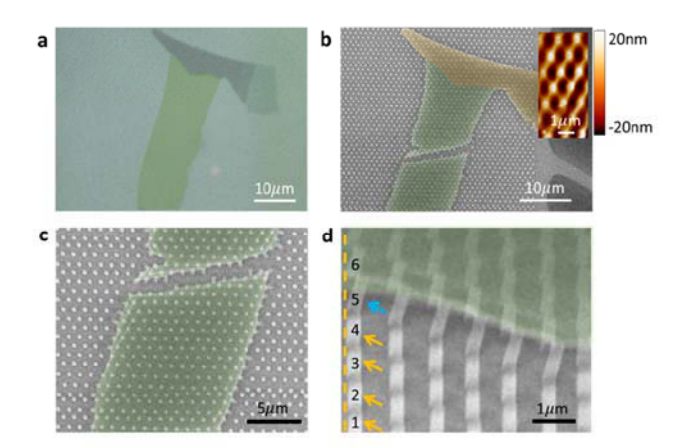


Figure 2. SEM images of graphene on LOR pillars. (a) Optical micrograph of graphene transferred on the LOR surface with prepatterned pillars (details in main text). Dark-gray and green colors indicate multilayer and single layer graphene, respectively. (b) SEM top view of the sample in (a) with LOR pillars seen as bright spots. Inset: AFM topography of graphene covering the pillars illustrates the sagging of the graphene layer in between pillars as well as the network of ripples formed along the symmetry directions of the pillar array. (c) High-resolution SEM image of the sample clearly shows the tear caused by the large strain. (d) A 45° angle side view shows bending of the LOR pillars supporting the edge of graphene membrane. Yellow dashed line indicates original orientation of the LOR pillars. Numbers designate the pillar rows. Note that pillars not covered by the graphene membrane, rows 1-4, are undistorted (yellow arrows). Pillars in row 5 and above that are situated under the graphene canopy are bent (blue arrow).

The bent pillars shed light on the response of the system to the strain induced by the collapse of the structure. One would expect the strain to be released by the graphene sheet sliding off the pillars. Instead, it appears that graphene is firmly anchored to the pillars via the van der Waals force and that part of its strain is released by bending the pillars. This scenario can only happen at the edges of the flake where the strain is asymmetric. However, in the center where no such release mechanism is available, once the strain exceeds the breaking point the flake must tear as is illustrated in Figure 2b. The bent LOR pillars technique presented here provides a direct and compelling visualization of the strain pattern.

We now turn to STM measurements for characterizing the local strain. Here we used an Au pillar array (70 nm height and $2 \mu m$ period) supported on an hBN flake instead of LOR for better surface cleanliness. The hBN flake was exfoliated on the SiO₂ surface and spin-coated with a thin layer of PMMA. Subsequently standard lift-off lithography was used starting with SEM exposure and development followed by Au/Ti (70 nm) deposition, and finally PMMA removal with acetone and isopropyl. The pillared substrate was further annealed in forming gas at 230 °C for 3 h to remove the PMMA residue before stacking the graphene on top. Au electrodes were added at the periphery of the graphene flake to clamp it down and avoid slippage. Figure 3a shows an SEM image of graphene on the Au-pillared substrate. To explore the strain effect, we first focus on the STM topography of an unstrained region of graphene lying outside the pillar array (Figure 3b). The small sample area was located by employing a capacitive navigation technique and a guiding electrode pattern. This technique is extremely efficient for finding small samples in the absence of optical access rapidly and without damaging the tip or sample.

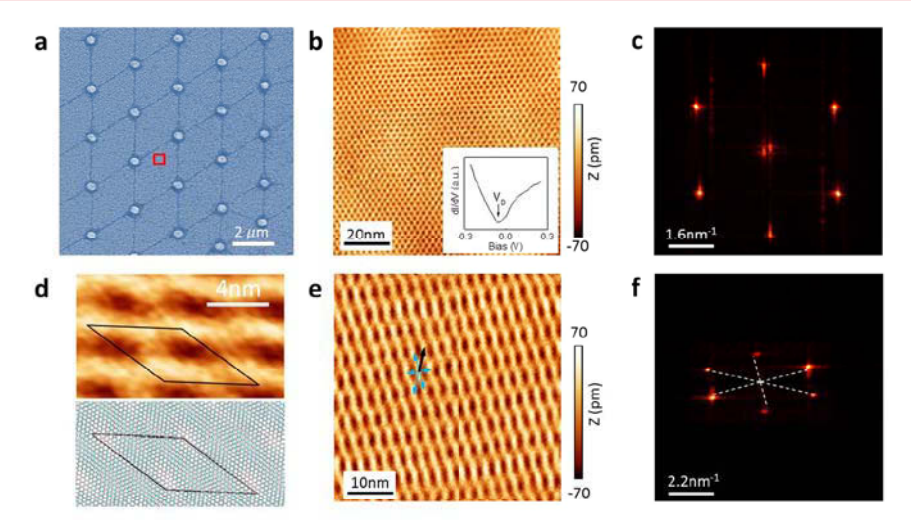


Figure 3. Imaging the distorted moiré pattern in graphene. (a) SEM image of the graphene/Au pillars (white spots) and the strain-induced ripples (lines connecting the pillars). (b,c) STM topography and fast Fourier transform (FFT) pattern of flat graphene far from the pillar area. The superlattice corresponds to the moiré pattern formed between graphene and the hBN flake, $V_b = -300$ mV, I = 20pA. Inset: dI/dV curve on flat graphene in (b) shows the characteristic "V" shape of unstrained graphene. (d) Comparison between measured distorted moiré pattern on strained graphene (top) and simulated model (bottom) as described in the text. The unit cell is shown in both panels. (e,f) Distorted moiré pattern and its FFT produced by the strained graphene lattice and the hBN substrate at the position marked by the red square (a). Arrows indicate the set of six lattice vectors of distorted ghraphene A_m is described in the text.

Outside the pillar array, we observe an undistorted moiré pattern of period 2.7 nm that corresponds to a twist angle of 5° between the graphene and hBN lattices. The undistorted moiré pattern signifies the absence of strain. This is further confirmed by the perfectly hexagonal Fourier transform pattern of the image in Figure 3c. The dI/dV spectrum in this region is "V" shaped again, consistent with unstrained graphene²⁵ (inset of Figure 3b).

We next consider the STM measurements taken within the pillared region. Here we observe a distorted moiré pattern (Figure 3e) and its fast Fourier transform (FFT) (Figure 3f), indicative of a strain-induced graphene lattice distortion. For unstrained graphene stacked on hBN, the slight mismatch between the two honeycomb lattices creates a moiré superstructure with perfect hexagonal symmetry^{23,24} (Figure 3b,c). If the graphene lattice is distorted, the resulting moiré pattern loses its hexagonal symmetry and the pattern is significantly altered²⁶ as is clearly seen in the topography (Figure 3d,e) as well as in its FFT (Figure 3f) (SI). A moiré pattern is very useful in this case because it can serve as a highly effective magnifying glass of strain-induced lattice distortions.¹⁴

To extract the strain from the distorted moiré pattern, we consider a model where a strained graphene lattice is superposed on an unstrained hBN crystal substrate. In this case the distorted superlattice Bragg vectors can be obtained using an elegant analytic expression: ${}^{14}\mathbf{G}_m = \frac{4\pi(\delta'^2 + \theta^2 - w'^2)}{\sqrt{3}a^2} \mathbf{I}_z \times \mathbf{A}_m$, where $\mathbf{I} = (\mathbf{I}_x) \mathbf{I}_x$ is the principal axis direction of the strain tensor, $\theta \ll 1$ rad is the misalignment angle between the two lattices, $\delta = 1.8\%$ is the lattice mismatch between unstrained graphene and the hBN substrate. The strained lattice mismatch $\delta' = \delta - w(1 - \sigma)/2$, depends on the strain magnitude, w, the Poisson ratio in graphene, ${}^{27}\sigma = 0.165$, and $w' = -w(1 + \sigma)/2$. Here $\mathbf{A}_m = \hat{M}a_m$ are the lattice vectors of the distorted superlattice $\delta' + (\mathbf{I}_x - \mathbf{I}_x)w' = 0.2\mathbf{I}_x\mathbf{I}_xw'$

$$\hat{M} = \frac{1}{\delta'^2 + \theta^2 - w'^2} \begin{pmatrix} \delta' + (l_y^2 - l_x^2)w' & \theta - 2l_x l_y w' \\ -\theta - 2l_x l_y w' & \delta' + (l_y^2 - l_x^2)w' \end{pmatrix} de$$

fines the transformation which magnifies and distorts the original graphene lattice, and \mathbf{a}_m is the set of six lattice vectors of undistorted ghraphene that are obtained by $m\pi/3$ rotations of $\mathbf{a}_0 = (\mathbf{a}, 0)$ with a = 0.246 nm, the lattice constant, and m = 0.1,...5.

Solving for the measured values of G_m in Figure 3f (dashed lines) we obtain $\theta = 0.07$ rad and w = 4.5%, resulting in a magnification, $M \sim 20$, for the largest lattice vector of the distorted lattice (black arrow in Figure 3e).

To verify the validity of the calculation we numerically superpose a distorted graphene lattice on an hBN substrate, where the distortion is calculated using the parameters $\theta=0.07$ rad, w=4.5% and $\sigma=0.165$. The resulting distorted superlattice moiré pattern, shown in the bottom panel of Figure 3d, closely resembles the measured one shown in the top panel. Significantly, although such a small distortion would be very difficult to detect in an isolated graphene sheet unless using a state of the art STM machine, the 20-fold magnification afforded by the moiré pattern makes the distortion readily detectable even with standard STM resolution. Indeed, earlier STM experiments on a MoS $_2$ layer strained by a pillared substrate 16 were not able to discern the lattice distortion or the presence of a PMF even though Raman spectra showed the presence of strain.

Considering the dI/dV spectrum in the distorted region (Figure 4a) we note that it no longer resembles the featureless "V" shape expected in unstrained graphene. Instead, the spectrum consists of a series of peaks suggesting the presence of a PMF which we discuss next. A strain induced PMF can arise when the nearest neighbor hopping parameters are modified. This introduces a pseudovector potential term, \vec{A} , in the Dirac-Weyl Hamiltonian describing the low energy excitation of graphene²⁸ (SI). In the limit of small atomic displacements, $u \ll a$: $A_x \sim \phi_0 \frac{\beta}{a} (u_{xx} - u_{yy})$; $A_y \sim \phi_0 \frac{\beta}{a} 2u_{xy}$, where $\phi_0 = \frac{h}{\epsilon}$ is the fundamental unit of flux, $u_{ij}(x, y)$ is the 2D strain field with the x axis taken along the zigzag direction of

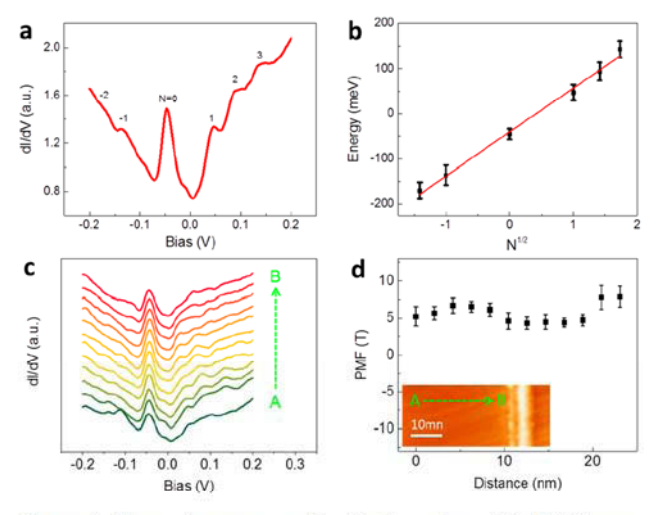


Figure 4. Electronic structure of strained graphene. (a) dI/dV curve for graphene observed near the ripple (red square in Figure 3a), $V_{\rm b}=-300\,$ mV, $I=20{\rm pA},\ V_{\rm g}=-10\,$ V. Peaks are labeled by their corresponding LL index. (b) Linear fit to eq 1 of peak energy versus square-root of LL index N from which we obtain the PMF value $B=(7.7\pm1)\,$ T. (c) Spatial dependence of the dI/dV curves along the direction perpendicular to the ripple. Same parameters as (a). (d) PMF values versus distance from the ripple extracted from the dI/dV curves in (c). The green arrow from A to B (23.1 nm) corresponds to the position of the spectra in (c).

the graphene lattice, and $\beta = -\partial \ln t/\partial \ln a I_{a=a_0} \sim 3.4$ relates the change in the hopping amplitude to the bond length. The pseudovector potential gives rise to a PMF, $\vec{B} = \overrightarrow{\nabla} \times \vec{A}$, normal to the graphene plane. Unlike a real magnetic field, the strain-induced PMF has opposite signs for graphene's two valleys, consistent with the fact that elastic deformations do not violate the time-reversal symmetry of the crystal. The PMF gives rise to a sequence of quantized PLLs similar to those produced by an external magnetic field

$$E_{\rm n} - E_{\rm D} = {\rm sgn}(N) v_{\rm F} \sqrt{2e\hbar B|N|}$$
 $N = 0, \pm 1, \pm 2, ...$ (1)

Here, $E_{\rm D}$ is the Dirac point energy, N is the level index, and $\nu_{\rm F}$ is the Fermi velocity.

In order to quantify the PMF in the strained graphene sample we label the peak sequence in the STS spectrum starting from N=0 which is taken close to the Dirac point in the unstrained lattice as shown in Figure 4a. The linear dependence of the peak energies on $N^{1/2}$ shown in Figure 4b, supports the interpretation of the peaks in terms of PLLs. Fitting the sequence to eq 1 and assuming $\nu_{\rm F}=1.0\times 10^6$ m/s, we obtain $B\sim (7.7\pm 1)$ T. Plotting the spectra and PMF along a line perpendicular to a fold (Figure 4c,d) we find the average PMF in this region, $B_{\rm PMF}\sim (6\pm 2)$ T.

We next compare the value of the PMF obtained from the PLL sequence to that expected from the strain-induced lattice distortion measured with the STM topography. An order of magnitude estimate of the strain-induced PMF can be obtained by assuming a triaxial strain configuration, 12,30 $B \approx \frac{\hbar}{\epsilon} \frac{8\beta \omega}{aD}$. Taking the size of the strained area as the disc of diameter $D \sim 1000$ nm, enclosed by the triangle of folds connecting three pillars, and using the strain value $w \sim 4.5\%$, we obtain an estimate of $B \sim 3.2$ T, consistent with the value obtained from the PLL sequence.

Previous reports of strain-induced PLLs employed STS measurements on graphene nanobubbles. S,31 In these reports, the strain was tightly localized on the bubble and relaxed outside it. In contrast to the bubble geometry, the in-plane strain configuration realized here makes it possible to delocalize the strain-induced PMF so that it is observed at distances that are hundreds of nanometers away from the nanopillar source. Importantly, the pillared device configuration for introducing strain is compatible with standard device fabrication methods, the only requirement being the prepatterned substrate.

In summary, we have studied strain-effects in a graphene membrane in contact with an hBN substrate and stretched by an array of nanopillars. The induced strain was directly visualized in STM and quantified through the magnifying effect of the moiré pattern formed against the hBN substrate. STS measurements revealed a sequence of PLL peaks in the DOS consistent with the strain-induced PMF. This work provides a quantitative comparison between the measured local strain and the induced PMF and demonstrates the possibility of modifying graphene's electronic band-structure by mechanical means rather than by chemical functionalization. Moreover, it introduces a new pathway for engineering the band structure and for realizing exotic transport properties 7,32 by patterning devices with preprogrammed PMFs.

ASSOCIATED CONTENT

S Supporting Information

The Supporting Information is available free of charge on the ACS Publications website at DOI: 10.1021/acs.nanolett.6b05228.

Description of the sample fabrication method for graphene on LOR pillars, additional data on undistorted and distorted moiré patterns with different pillar configurations, more information about modeling the distorted moiré pattern, and additional data about strain-induced pseudomagnetic fields (PDF)

AUTHOR INFORMATION

Corresponding Authors

*E-mail: jhmao@physics.rutgers.edu (J.M.).

*E-mail: eandrei@physics.rutgers.edu (E.Y.A.).

ORCID 6

Eva Y. Andrei: 0000-0002-2516-2749

Author Contributions

§Y.J. and J.M. contributed equally to this work.

Notes

The authors declare no competing financial interest.

ACKNOWLEDGMENTS

E.Y.A., J.M., and X.L. acknowledge support from DOE-FG02-99ER45742, Y.J. and J.D. acknowledge support from NSF-DMR 1207108

ABBREVIATIONS

PMF, pseudomagnetic field; PLLs, pseudo Landau levels; hBN, hexagonal boron nitride; STM, scanning tunneling microscopy; STS, scanning tunneling spectroscopy; AFM, atomic force microscopy; SEM, scanning electron microscopy; LDOS, local density of states; Au, gold; Ti, titanium; 2D, two dimension; SiO₂, Silicon oxide; FFT, fast Fourier transform

■ REFERENCES

(1) Castro Neto, A. H.; Guinea, F.; Peres, N. M. R.; Novoselov, K. S.; Geim, A. K. Rev. Mod. Phys. **2009**, 81 (1), 109–162.

- (2) Andrei, E. Y.; Li, G. H.; Du, X. Rep. Prog. Phys. 2012, 75 (5), 056501.
- (3) Ferrari, A. C.; et al. Nanoscale 2015, 7 (11), 4598-4810.
- (4) Lee, C.; Wei, X. D.; Kysar, J. W.; Hone, J. Science **2008**, 321 (5887), 385–388.
- (5) Masir, M. R.; Moldovan, D.; Peeters, P. M. Solid State Commun. 2013, 175-176, 76-82.
- (6) Vozmediano, M. A. H.; Katsnelson, M. I.; Guinea, F. Phys. Rep. 2010, 496 (4–5), 109–148.
- (7) Carrillo-Bastos, R.; León, C.; Faria, D.; Latgé, A.; Andrei, E. Y.; Sandler, N. Phys. Rev. B: Condens. Matter Mater. Phys. 2016, 94 (12), 125422.
- (8) Levy, N.; Burke, S. A.; Meaker, K. L.; Panlasigui, M.; Zettl, A.; Guinea, F.; Neto, A. H. C.; Crommie, M. F. Science **2010**, 329 (5991), 544–547.
- (9) Tomori, H.; Kanda, A.; Goto, H.; Ootuka, Y.; Tsukagoshi, K.; Moriyama, S.; Watanabe, E.; Tsuya, D. Appl. Phys. Express 2011, 4 (7), 075102.
- (10) Reserbat-Plantey, A.; et al. Nano Lett. 2014, 14 (9), 5044-5051.
- (11) Choi, J.; Kim, H. J.; Wang, M. C.; Leem, J.; King, W. P.; Nam, S. Nano Lett. **2015**, 15 (7), 4525–4531.
- (12) Guinea, F.; Katsnelson, M. I.; Geim, A. K. Nat. Phys. 2010, 6 (1), 30-33.
- (13) Neek-Amal, M.; Covaci, L.; Peeters, F. M. Phys. Rev. B: Condens. Matter Mater. Phys. 2012, 86 (4), 041405.
- (14) Cosma, D. A.; Wallbank, J. R.; Cheianov, V.; Fal'ko, V. I. Faraday Discuss. **2014**, 173, 137–143.
- (15) Dean, C. R.; et al. Nat. Nanotechnol. 2010, 5 (10), 722-726.
- (16) Li, H.; et al. Nat. Commun. 2015, 6, 7381.
- (17) Hure, J.; Roman, B.; Bico, J. Phys. Rev. Lett. 2012, 109 (5), 054302.
- (18) Yu, T. X.; Stronge, W. J. Int. J. Solids Struct. 1985, 21 (10), 995–1003.
- (19) Pocivavsek, L.; Dellsy, R.; Kern, A.; Johnson, S.; Lin, B. H.; Lee, K. Y. C.; Cerda, E. *Science* **2008**, 320 (5878), 912–916.
- (20) Paulsen, J. D.; Hohlfeld, E.; King, H.; Huang, J.; Qiu, Z.; Russell, T. P.; Menon, N.; Vella, D.; Davidovitch, B. *Proc. Natl. Acad. Sci. U. S. A.* **2016**, *113* (5), 1144–1149.
- (21) Mao, J. H.; Jiang, Y. H.; Moldovan, D.; Li, G. H.; Watanabe, K.; Taniguchi, T.; Masir, M. R.; Peeters, F. M.; Andrei, E. Y. *Nat. Phys.* **2016**, *12* (6), 545.
- (22) Li, G.; Luican, A.; Andrei, E. Y. Rev. Sci. Instrum. 2011, 82 (7), 073701.
- (23) Yankowitz, M.; Xue, J. M.; Cormode, D.; Sanchez-Yamagishi, J. D.; Watanabe, K.; Taniguchi, T.; Jarillo-Herrero, P.; Jacquod, P.; LeRoy, B. J. *Nat. Phys.* **2012**, *8* (5), 382–386.
- (24) Decker, R.; Wang, Y.; Brar, V. W.; Regan, W.; Tsai, H. Z.; Wu, Q.; Gannett, W.; Zettl, A.; Crommie, M. F. *Nano Lett.* **2011**, *11* (6), 2291–2295.
- (25) Luican, A.; Li, G.; Andrei, E. Y. Solid State Commun. 2009, 149 (27–28), 1151–1156.
- (26) Summerfield, A.; et al. Sci. Rep. 2016, 6, 34474.
- (27) Politano, A.; Chiarello, G. Nano Res. 2015, 8 (6), 1847-1856.
- (28) Amorim, B.; et al. Phys. Rep. 2016, 617, 1-54.
- (29) Moldovan, D. Ph.D. Thesis, Universiteit Antwerpen, Antwerpen, Belgium, 2016.
- (30) Guinea, F.; Geim, A. K.; Katsnelson, M. I.; Novoselov, K. S. Phys. Rev. B: Condens. Matter Mater. Phys. 2010, 81 (3), 035408.
- (31) Lu, J.; Neto, A. H. C.; Loh, K. P. Nat. Commun. 2012, 3, 823.
- (32) Phillips, M.; Mele, E. J. 2017 eprint arXiv:1701.06490.